Textures and Microstructures, Vol. 32, pp. 369–381
Reprints available directly from the publisher
Photocopying permitted by license only

THE TEXTURE AND CREEP ANISOTROPY OF FUEL ELEMENT SHELLS MANUFACTURED FROM Cr16Ni15Mo3Ti TYPE STEELS

V.N. KUZNETSOV, O.N. KHAKIMOVA, V.I. SHALAEV*, N.F. VIL'DANOVA, V.V. SAGARADZE and YU.I. FILIPPOV

Institute of Metal Physics, Ural Division of the Russian Academy of Sciences, 18, S. Kovalevskaya street, 620219, Ekaterinburg, Russian Federation

(Received in final form 28 September 1997)

A study was undertaken into the structure, the texture, the strength, and the creep of the Cr16Ni15Mo3Ti type steel tubes cold-deformed to 20% strain that are used as the fuel element shells for fast-neutron reactors. The tubes were found to have fibrous ⟨111⟩ and ⟨100⟩ textures along their axis. The preferred orientations ⟨011⟩ normal to the radial plane and ⟨011⟩ and ⟨112⟩ normal to the plane tangential to the tube surface were determined. The strength, the creep strength, and the rupture strength proved to be higher along the tube axis. Qualitatively, this is attributed to a specific texture and the grain shape of the material.

Keywords: Austenitic stainless steel; Fuel element shell; Texture; Microstructure; Creep

INTRODUCTION

The austenitic stainless steels of the Cr16Ni15Mo3Ti type have been widely used as a material of fuel element shells for fast-neutron reactors (Chuev *et al.*, 1994) and continue to be very promising for this application (Sagaradze *et al.*, 1993). The tubes experience both tensile stresses along their axis and the internal pressure due to the swelling fuel and the fuel decay gas products (Samoilov *et al.*, 1982). It is therefore of special interest to examine the anisotropy of the mechanical properties

* Corresponding author.

of the tubes. Probably, different mechanical properties along and across the tube axis are determined by specific features of the texture, which are caused in part by cold deformation to 20% strain. The texture characteristics (intensity, scattering, and orientation ratio) generally vary over the cross section of tubes, sheets, or wire (Wassermann and Graeven, 1962) as a result of a nonuniform rolling deformation of the material. This paper is concerned with the study of the texture, its distribution over the height of the samples, and the effect of the texture on the strength, the creep strength, and the rupture strength of fuel element shells made of the Cr16Ni15Mo3Ti type steels.

EXPERIMENTAL

The subject of study was thin-walled shells (6.9 mm in diameter, with walls 0.4 mm thick) made from the Cr16Ni15Mo3Ti type steels cold-deformed to $20 \pm 3\%$. The chemical composition of these steels is given in Table I. The microstructure and the texture of the steels were examined in three mutually perpendicular planes: the surface and the transverse and longitudinal section planes (Fig. 1). The texture in the last two sections was studied on stacked samples comprising 20 plates each such that the surface of interest always measured at least 8 mm by 20 mm. Microsections for microscopic investigations were prepared by electropolishing at a d.c. voltage of 25 V in a solution containing 570 ml of orthophosphoric acid and 170 g of chromic anhydride. Electrolytic etching was done at a voltage of 10 V in a solution containing 10 ml of HNO_3 and 30 ml of HCl. The microstructure was examined in a Neophot-21 light microscope.

The texture was studied with a DRON-2.0 X-ray diffractometer using Mo K_α radiation and inverse pole figures. The integral intensity of the diffraction lines necessary for calculating the inverse pole figures was determined automatically from the number of pulses counted when

TABLE I The chemical composition of the Cr16Ni15Mo3Ti type steels

Alloy	*C*	*Mn*	*S*	*P*	*Cr*	*Ni*	*V*	*Ti*	*Si*	*Al*	*Co*	*Mo*	N_2	*B*
1	0.06	1.6	0.08	0.07	16.2	14.3	0.15	0.4	0.4	—	0.005	2.2	0.013	0.001
2	0.029	0.38	0.05	0.015	15.95	15	—	1.02	0.5	0.08	—	2.53	—	—

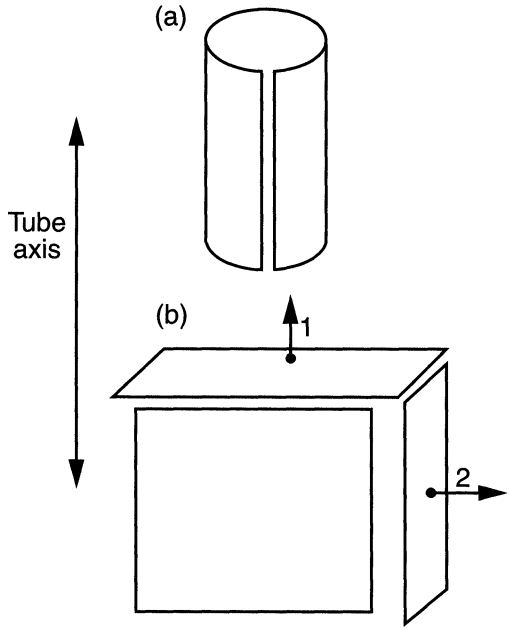

FIGURE 1 Blanks of the samples: (a) after cutting out from a tube and (b) after spreading to a sheet. (1) is the cross section and (2) is the longitudinal section of the tube wall.

every line was scanned at a constant rate over the entire angle interval of the diffraction maximum, minus the background count. In ascertaining the homogeneity of the texture over the cross section of a tube, inverse pole figures were constructed, starting from the outer surface each time a layer 50 μm thick was removed from the tube.

The anisotropy of the mechanical properties was assessed on small nonstandard samples measuring $0.4 \times 3 \times 20$ mm, which were prepared from short tubes (see Fig. 1). The tube was slit, spread by hand and straightened between flat rolls without any change in thickness accurate to ± 0.01 mm. The uneven edges of the plates were ground so that the test samples had a rectangular cross section. The yield stress σ_{02}, the tensile strength σ_B, the specific elongation δ, and the reduction of area ψ were measured on a ZD-10/90 tensile testing machine at 20°C, making three tests for each orientation of the samples.

The anisotropy of the creep strength and that of the rupture strength were studied on flat samples prepared in accordance with the procedure

described above. The difference was that reinforcing bars having pin holes, whose centers were aligned (accurate to within $\pm 0.1°$) with the sample's axis, were spot-welded to the grip pads of these samples. The creep tests were made in air at a temperature of 650°C on an AIMA-5-2 machine with the samples loaded uniaxially. The test temperature and the test load were maintained constant to within $\pm 3°$ and $\pm 1\%$ respectively.

RESULTS AND DISCUSSION

The microstructure of the steel 2 in three mutually perpendicular sections is shown in Fig. 2. In the cross section of the tube wall the grains

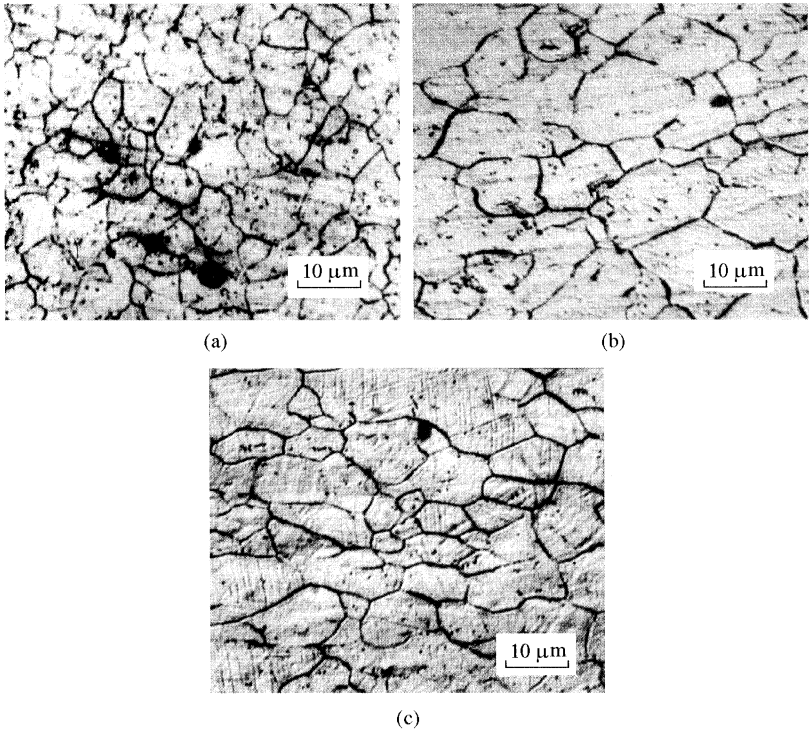

(a) (b)

(c)

FIGURE 2 Microstructure of the steel 2: (a) cross section of the tube wall; (b) longitudinal section of the tube wall; (c) the tube surface.

are equiaxial and measure about 6 μm (see Fig. 2(a)). In the longitudinal section and in the plane parallel to the tube surface the grains are extended along the tube axis and measure about 9 μm in this direction (see Fig. 2(b) and (c)). Thus, in the unit volume the grain boundaries are nearly 1.5 times longer in the direction of the tube axis than they are in the perpendicular direction. The microstructure of the steel 1 in three mutually perpendicular directions is analogous to that of the steel 2.

The inverse pole figure in the transverse plane (Fig. 3(a)) suggests the presence of two well-defined maxima ⟨111⟩ and ⟨100⟩ having the density of 4.45 and 3.76 respectively. This means that two groups of fcc crystallites exist: in one group the body diagonal and in the other a cube edge is parallel to the tube axis. For the steel 1 the inverse pole figures are similar (see Fig. 3(c) and (d)). This kind of texture is typical of drawn fcc metals and alloys having a medium stacking fault energy (SFE) (Honeycombe, 1968). For example, in the case of copper whose SFE

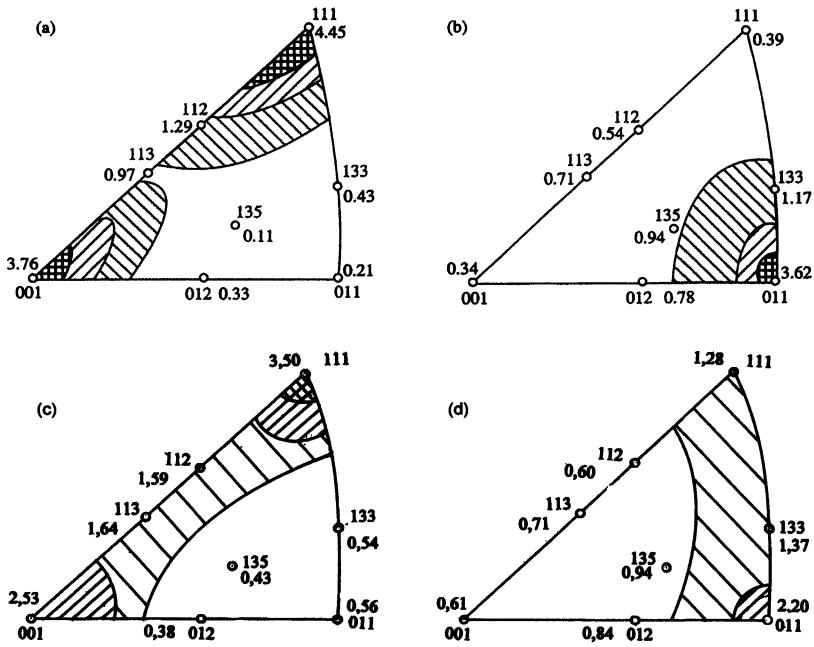

FIGURE 3 Inverse pole figures taken at (a) the cross section and (b) the longitudinal section of the wall of a tube made from the Cr16Ni15Mo3Ti type steel.

(70 mJ/m^2(Zolotarevskii, 1983)) is close to that of the Cr16Ni15Mo3Ti type steel (calculated 70 mJ/m^2 and experimental 55 mJ/m^2 (Konobeev and Rudnev, 1983)), only 10% of the crystallites deviate from the ⟨111⟩ or ⟨100⟩ orientation when the copper wire is drawn from 3 mm to 0.3 mm in diameter (Wassermann and Graeven 1962).

A fibrous texture is also typical of tubes when their diameter and wall thickness are reduced to the same extent during rolling (Wassermann and Graeven, 1962). This situation persists as long as the reduction ratio between the wall thickness and the diameter is less than 2. When this reduction ratio exceeds 2.5, the sheet texture appears in the material. The initial pierced tube billet had a diameter of 102 mm with walls 12 mm thick. The fabrication of the fuel element cladding tubes to the prefinished condition involved seven operations. The ratio in question was not greater than 1.48 in each of the operations. Every operation was followed by recrystallization annealing. In certain instances annealing does not cause fundamental changes in the texture produced by rolling (Wassermann and Graeven, 1962). Therefore a prefinished tube should have a fibrous texture of the ⟨111⟩ and ⟨100⟩ types. The finishing operation involved cold working to 20% of a billet 7.6 mm in diameter with walls 0.46 mm thick. This amount of straining could not incur radical changes in the existing texture, because the wall thickness/diameter reduction ratio was close to unity. The same reduction in the wall thickness and the diameter produced almost equiaxial grains in the cross section of the tube wall, which were extended along the tube axis.

As opposed to wire, the tubes do not develop a texture characterized by a full rotation of the crystallographic directions about the fiber axis. For example, in rolled copper tubes (Wassermann and Graeven, 1962) a ⟨011⟩ orientation normal to the plane tangential to the tube surface was observed in addition to the ⟨111⟩ and ⟨100⟩ orientations parallel to the tube axis. In the steel 2, also, the preferred ⟨011⟩ and ⟨112⟩ orientations with a density of 2.94 and 1.44 respectively were observed normal to the tangential plane (Fig. 4(a)). Moreover, a ⟨011⟩ direction with a density of 3.62 is realized normal to the radial plane (see Fig. 3(b)). The density of this direction in the steel 1 is slightly less (see Fig. 3(c)).

Figure 4(a)–(e) show the changes observed in the inverse pole figures taken from the outer and inner surfaces and also at certain depths from the surfaces of a tube made from the steel 2. The intensity of the ⟨112⟩ component continuously decreases until it vanishes completely after

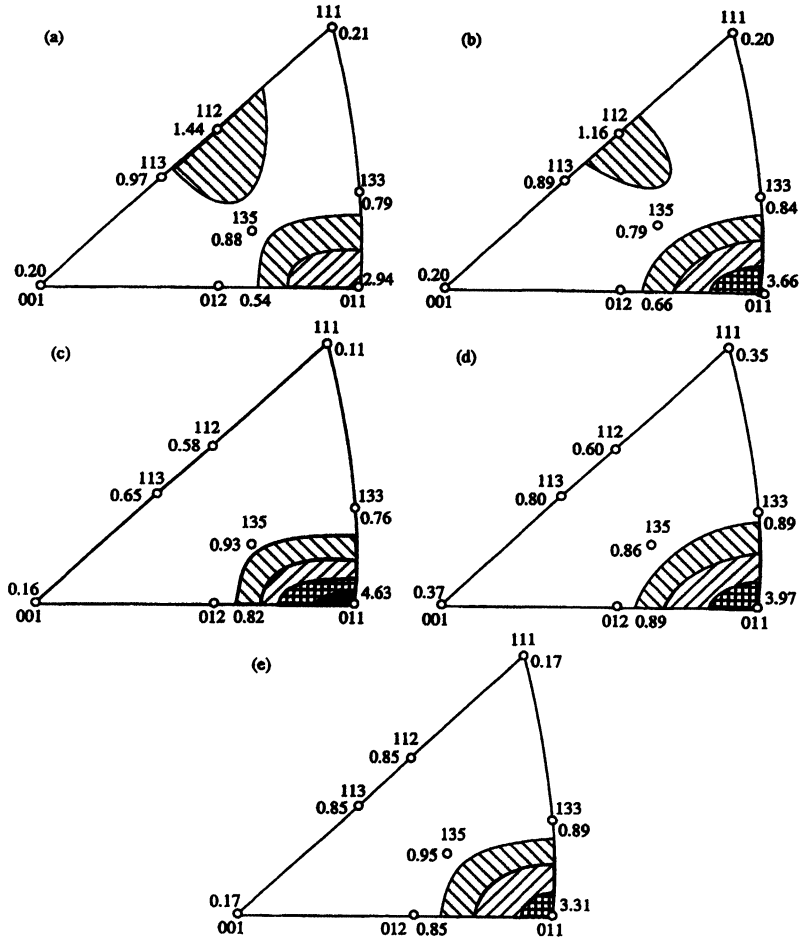

FIGURE 4 Inverse pole figures taken in the plane parallel to the surface of the steel 2 tube: (a) the outer tube surface; (b) a depth of 50 μm from the outer surface; (c) a depth of 100 μm from the outer surface; (d) a depth of 140 μm from the outer surface; and (e) the inner surface of the tube.

a 100-μm layer is removed from the outer surface. The intensity of the ⟨011⟩ component attains a maximum of 4.63 (see Fig. 4(c)) and the scattering falls to its lowest. The last component weakens if more of the surface layer is removed (140 μm). When still more stock is etched off the surface, neither the mix of the texture components nor the intensity of the ⟨011⟩ component changes. The form of the inverse pole figures

on the outer and inner surfaces of the tubes fabricated from steel 1 differs little from that of steel 2.

The presence of the preferred ⟨112⟩ orientation (in addition to ⟨011⟩) in a thin layer near the outer surface of the tube is probably due to a greater strain of the material at the point of its contact with the tool. As a result, the reduction ratio between the wall thickness and the diameter exceeds 2.5 and the sheet texture is realized (Wassermann and Graeven, 1962).

Thus, the Cr16Ni15Mo3Ti steel tubes 6.9 mm in diameter with walls 0.4 mm thick cold-deformed to 20% strain have a fibrous texture with the ⟨111⟩ and ⟨100⟩ directions along the rolling axis. Also, a preferred ⟨011⟩ orientation normal to the radial plane and preferred ⟨011⟩ and ⟨112⟩ orientations in the plane tangential to the tube surface exist. The last orientation disappears at a depth of 100 μm from the outer surface.

The mechanical test results for the steel 2 at 20°C are summarized in Table II. Note that the samples cut out along the tube axis have a higher strength ($\sigma_{0.2}$ and σ_b) and a lower ductility (δ and ψ) than the transverse samples.

By way of example, Fig. 5 presents creep curves for the steel 2 samples at $\sigma = 200$ MPa and $T = 650$°C. One may see that the time to rupture of the samples oriented along the tube axis is longer than that of the samples oriented across the tube axis. This difference persists over the entire range of loads ($170 \leq \sigma \leq 300$ MPa) (Fig. 6). At $\sigma = 170$ MPa the steady-state creep rate $\dot{\varepsilon}$ of the samples oriented across the tube axis is 1.5 higher than $\dot{\varepsilon}$ measured for the samples oriented along the tube axis. Given this value of σ, the difference in the time to rupture τ amounts to 37% ($\tau_{\parallel} > \tau_{\perp}$).

Figure 6(c) shows a graph relating the long-term ductility ε_r to the stress. One may see that ε_r of the samples oriented along the tube axis is always higher than its counterpart for the transverse-oriented samples. At the lowest stress $\sigma = 170$ MPa, the dependence reverses. Samples of the steel 1 were tested at the same temperature $T = 650$°C but in a wider

TABLE II Mechanical properties of the steel 2 samples cut out along and across the tube axis, as measured at 20°C

Direction relative the tube axis	$\sigma_{0.2}$ (MPa)	σ_B (MPa)	δ (%)	ψ (%)
Along	841	896	18.6	37.4
Across	795	867	21.0	38.3

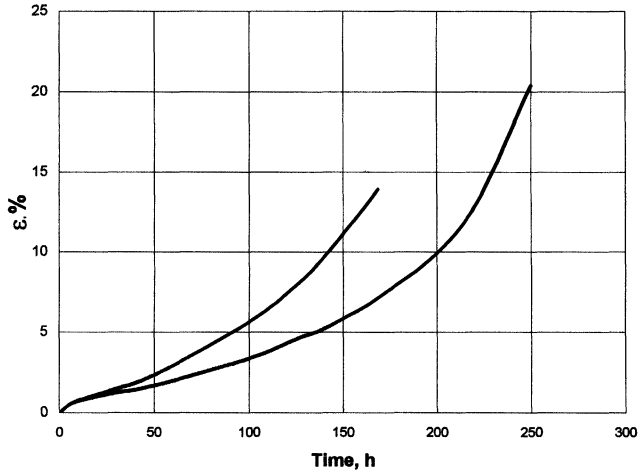

FIGURE 5 Creep curves of the steel 2 samples cut out (1) along and (2) across the tube axis. The curves were registered at a temperature of 650°C and a stress of 200 MPa.

interval of stresses ($127 < \sigma < 367$ MPa). The corresponding test results are presented in Fig. 7. It may be seen that they are qualitatively similar to those obtained for the steel 2. Quantitatively the values of $\dot{\varepsilon}$ and τ differ little but those of ε_r differ considerably. The main difference with respect to ε_r is that its values for the samples oriented along and across the tube axis become nearly equal at stresses much lower than those for the steel 2 samples.

All these mechanical properties may be accounted for by specific features of the texture of the tubes and the grain shape of the steel. As was discussed in the foregoing, most crystallites along the tube axis and, consequently, in the longitudinal samples are oriented in the $\langle 111 \rangle$ and $\langle 100 \rangle$ directions. In the transverse samples the tensile axis goes across the tube axis and most crystallites along the sample's axis extend in the $\langle 110 \rangle$ direction (see Figs. 3 and 4). If a textured polycrystal is assumed in the first approximation to be an analog of a single crystal, then, according to Borodkina and Spektr (1968), at room temperature the orientations close to [111] are the "hardest" and those close to [110] are the "softest". Deformation of crystals with soft orientations begins and continues at minimum stresses thanks to a favorable orientation of the primary slip system. For this reason, they have a long first stage of deformation and a

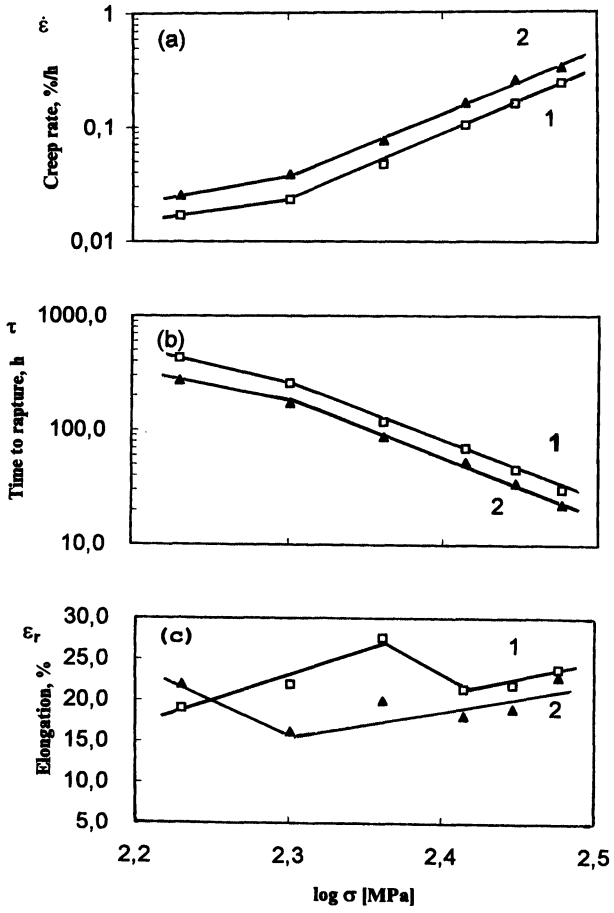

FIGURE 6 Stress dependence of (a) the steady-state creep rate $\dot{\varepsilon}$, (b) the time to rupture τ, and (c) the long-term ductility ε_r for the steel 2 samples cut out (1) along and (2) across the tube axis, as measured at 650°C.

low work-hardening rate. For example, during the first stage of tension the work-hardening rate of single crystals of copper (Honeycombe, 1968), whose SFE is close to that of the steel in question (Honeycombe, 1968; Konobeev and Rudnev, 1983), is 51–117 MPa at orientations near [111], 41 MPa near [100], and 10–34 MPa near [110]. In addition, the [111] and [100] directions in copper single crystals are associated with a markedly greater cleavage stress and a higher work-hardening rate

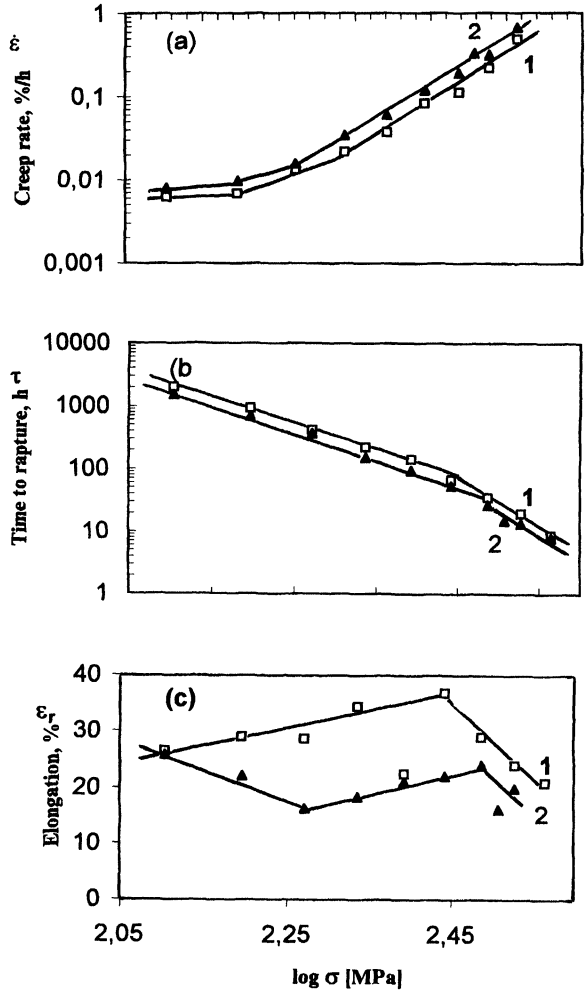

FIGURE 7 Stress dependence of (a) the steady-state creep rate $\dot{\varepsilon}$, (b) the time to rupture τ, and (c) the long-term ductility ε_r for the steel 1 samples cut out (1) along and (2) across the tube axis, as measured at 650°C.

during the first and, what is especially significant for polycrystals, the second stage (Honeycombe, 1968), compared to the [110] and [112] directions.

Most crystallites in the longitudinal samples are oriented in the ⟨111⟩ and ⟨100⟩ directions along the sample's axis. Therefore these samples

should have a higher resistance to plastic deformation than the transverse samples whose axis coincides with the ⟨110⟩ direction. This explains why the samples oriented along and across the tube axis exhibit different mechanical properties.

Specific features of the texture formation account for different ductility of the Cr16Ni15Mo3Ti type steels subject to cold deformation along and across the tube axis. The specific elongation of the transverse samples is regularly higher than that of the longitudinal samples (Table II). This fact is probably due to a lower yield stress and, consequently, a greater specific elongation needed for the voids to coalesce (Knott, 1979).

During creep, the transverse samples have a lower ductility than the longitudinal samples. Most likely, this is because the contribution from grain-boundary defects (such as voids and cracks) is the higher, the longer the boundaries perpendicular to the tensile axis (Knott, 1979). The examination of the microstructure shows (see Fig. 2) that these boundaries are nearly 1.5 times longer in the transverse samples and therefore they have a greater probability of fracture under a lower total strain.

CONCLUSIONS

1. Tubes 6.9 mm in diameter with walls 0.4 mm thick fabricated from the Cr16Ni15Mo3Ti type steels and cold deformed to a strain of 20% were found to have a fibrous texture, the preferred orientations along the rolling axis being ⟨111⟩ and ⟨100⟩. Other preferred orientations are ⟨011⟩ normal to the radial plane and ⟨011⟩ and ⟨112⟩ normal to the plane tangential to the tube surface. The last orientation disappears at a depth of 100 μm from the outer surface.
2. The strength, the creep strength, and the rupture strength proved to be higher along the tube axis. This fact may be qualitatively attributed to the predominance of the ⟨111⟩ and ⟨100⟩ texture components in the axial direction and the ⟨011⟩ component in the lateral direction, and also to the grain shape.
3. Fibrous texture of tubes fabricated of Cr16Ni15Mo3Ti type steel is not optimal from the viewpoint of use as fuel element shells in fast-neutron reactor.

References

Borodkina, M.M. and Spektr, E.N. (1968). *Rentgenograficheska Analiz. Tekstury Metallov i Splavov* (*X-ray Diffraction Analysis of Texture in Metals and Alloys*), Moscow: Mir.

Chuev, V.V., Lanskih, B.N., Ogorodov, A.N. (1994). Rabotosposobnost TVS Bistrih Reactorov. In: *Issledovanie Konstrukzionnih Materialov Elementov Aktivnoy Zoni Bistrih Natrievich Reactorov*. Ural Division, Russian Academy of Science, Ekaterinburg, pp. 85–140.

Honeycombe, R. (1968). *The Plastic Deformation of Metals*, Cambridge: Cambridge Univ. Press.

Knott, J.F. (1979). *Fundamentals of Fracture Mechanics*, London: Butterworths.

Konobeev, Yu.I. and Rudnev, S.I. (1983) Assessing the stacking fault energy of frank loops in OKhl6NI5M3B stainless steel, *Atom. Energ.*, **53**(2), 107–108.

Sagaradze, V.V., Nalesnik, V.M., Lapin, S.S. *et al.* (1993). Precipitation hardening and radiation damageability of austenitic stainless steels, *J. Nucl. Mater.* **202**, 137–144.

Samoilov, A.G., Kashtanov, A.I., and Volkov, V.S. (1982). *Disperswnnye Tvely, Materialy i Tekhnologiya, Tom I* (*Dispersion Nuclear Fuel Elements, Materials and Fabrication Methods, Vol.* 1), Moscow: Energoizdat,.

Wassermann, G. and Graeven, J. (1962). *Texturen Metallischer Workstoffe*, Berlin: Springer,.

Zolotatevskii, V.S. (1983). *Mekhanicheskie Svoistva Metallov* (*Mechanical Properties of Metals*), Moscow: Metallurgiya,.